Photo-controlled Cargo Release from Dual Cross-linked Polymer Particles

Shereen Tan,[a] Jiwei Cui,[b] Qiang Fu,[a] Eunhyung Nam,[a] Katharina Ladewig,[a] Jing M. Ren, [a] Edgar H. H. Wong,[a] Frank Caruso,[b] Anton Blencowe,*[,c] Greg G. Qiao*[,a]

[a]Polymer Science Group, Department of Chemical and Biomolecular Engineering, The University of Melbourne, Parkville, VIC 3010, Australia.

[b]ARC Centre of Excellence in Convergent Bio-Nano Science and Technology, and the Department of Chemical and Biomolecular Engineering, The University of Melbourne, Parkville, Victoria 3010, Australia

[c]School of Pharmacy and Medical Sciences, Division of Health Sciences, The University of South Australia, Adelaide, SA 5001, Australia.

*e-mail: anton.blencowe@unisa.edu.au, gregghq@unimelb.edu.au

Abstract

Instantaneous burst release of a payload from polymeric particles upon photo-irradiation was engineered by altering the cross-linking density. This was achieved *via* a dual cross-linking concept whereby non-covalent cross-linking was provided by cyclodextrin host-guest interactions, and irreversible covalent cross-linking was mediated by continuous assembly of polymers (CAP). The dual cross-linked particles (DCPs) were efficiently infiltrated (~ 80-93%) by the biomacromolecule dextran (molecular weight up to 500 kDa) to provide high loadings (70-75%). Upon short exposure (5 s) to UV light, the non-covalent cross-links were disrupted resulting in increased permeability and burst release of the cargo (50 mol% within 1 s) as visualised by time-lapse fluorescent microscopy. As sunlight contains UV light at low intensities, the particles can potentially be incorporated into systems used in agriculture, environmental control, and food packaging, whereby sunlight could control the release of nutrients and antimicrobial agents.

Keywords: (cyclodextrin, supramolecular chemistry, particle, entrapment, delivery, polymerization)

Introduction

The fabrication and design of polymeric particles has seen intensive interest in both academia and industry due to their ability to encapsulate cargo and release their contents on demand under specific conditions.[1-2] The ability to encapsulate high loadings of cargo and controllably deliver their payload makes polymeric particles useful in a wide range of applications including, deodorant and antiperspirant release,[3-4] nutrient preservation,[5-6] drug delivery[7-8] and micro-reactors.[9-10] When engineering particle systems, stimuli-responsiveness is usually incorporated by either (i) alerting their permeability by fabricating them with responsive polymers (e.g., pH,[11-12] temperature,[13-14] oxidation,[15-16] light[17-18]) or (ii) by incorporating cross-linkers which render the particles susceptible to chemically induced disassembly.[19] The former has grown in popularity as the latter results in more complex synthetic protocols, and there is also a possibility for deleterious side-effects derived from degradation products.[1] However, in both cases, cargo release is often accompanied with the degradation of the polymeric carriers. This is arguably unfavourable in some applications, such as food packaging, where the degradation products can diffuse into the food.

The utilization of a dual cross-linked system, wherein the cross-linking density of the particles (*i.e.,* particle permeability) can be altered upon certain triggers can offer a route to develop carriers that do not degrade upon payload release. This technique is generally under explored with limited published research,[20-21] most likely due to technical difficulties associated with current fabrication methods; where a high level of cross-linking must be maintained in order for particles and capsules to be stable. Recently, our group reported the continuous assembly of polymers (CAP) approach; a facile, highly amendable approach to fabricate nanoscale cross-linked films and coatings

in a single-step strategy.[22] The CAP approach utilizes controlled polymerization protocols to polymerize macrocross-linkers – (bio)macromolecules with pendant polymerizable moieties – from initiator functionalized substrates.[23] The CAP approach is a versatile method for the fabrication of various functional nanocoatings, including superhydrophobic and switchable thin films[24], chiral stationary phases,[25] low-biofouling coatings[26] and compartmentalized micelle-based films.[27] When CAP mediated by ring-opening metathesis polymerization (CAP_{ROMP}) is applied to particle templates, only 7 mol % of pendant polymerizable groups are required to form stable replica particles in one-step after template dissolution.[23] This low percentage of cross-linking provides a handle for the preparation of covalently cross-linked particles in a facile and robust manner.

The use of cyclodextrin (CD) host-guest supramolecular interactions is a popular approach to impart non-covalent cross-links as their interactions are specific yet reversible.[28-29] CDs are cyclic oligosaccharides usually composed of six-to-eight D-glucose units. Owing to their hydrophobic cavity, CDs are able to form reversible interactions with appropriately sized guest molecules and polymers; if these guests undergo structural changes in response to light it is often possible to switch between the complexed and free states.[28-31] The utilization of CD host-guest interactions continues to expand, finding new applications for advanced functional materials[28-35] and sophisticated structures,[29, 36-37] including smart adhesives,[38-39] self-healing networks[40-41] and electrochemical actuators.[42]

Herein, we exploit the advantages of CAP_{ROMP} and CD host-guest interactions to engineer dual cross-linked particles (DCPs) with photo-responsiveness. In this process, specific yet reversible non-covalent cross-linking is achieved through CD-azobenzene

host-guest interactions, whilst irreversible covalent cross-linking is obtained through CAP_{ROMP}. The DCPs show size selectivity and can be efficiently infiltrated (~ 80-93 %) by high molecular weight dextrans; a model biomacromolecule. Short exposure (5 s) to UV irradiation (365 nm) results in disruption of the non-covalent cross-links, resulting in significant expansion of the particles, an increase in particle deformability, and cargo release. As direct sunlight contains UV light (~ 3 mW cm^{-3})[43] these carrier systems could potentially be used to deliver (bio)macromolecules/compounds without the presence of particle degradation products upon expose to sunlight. The technique outlined also opens up new avenues for the application of CD host-guest supramolecular systems.

Results and Discussion

To engineer DCPs *via* the CAP_{ROMP} approach two macrocross-linkers were initially prepared. Low-fouling poly(*N*-(2-hydroxyethyl)acrylamide) (pHEAm)[44] was chosen as the macrocross-linker backbone and synthesized by conventional free radical polymerization of the monomer *N*-(2-hydroxyethyl)acrylamide (HEAm). ^{1}H NMR spectroscopic analysis revealed ~ 92 % monomer conversion after 5 h by comparing resonances of the vinylic and hydroxyl protons (SI, **Figure S1a**). The number average molecular weight (M_n^{GPC}) was 12.9 kDa (with respect to poly(ethylene glycol) standards) with a dispersity index ($Đ$) of 1.84, as determined by gel permeation chromatography (GPC) (**Figure S1b**). Pendent polymerizable norbornene groups were then introduced onto the pHEAm backbone *via* partial esterification of the hydroxyl groups. ^{1}H NMR spectroscopic analysis revealed that 10 mol% of norbornene moieties (relative to repeat units) were conjugated onto the pHEAm. The macrocross-linker **P1** was subsequently synthesized *via* partial esterification of the remaining hydroxyl groups with an azobenzoic acid derivative, whereas macrocross-linker **P2** was prepared by conjugation of an alkyne derivative through esterification, followed by copper-catalyzed azide alkyne cycloaddition (CuAAC) with a mono-azide functional α-CD (**Scheme 1**). ^{1}H NMR spectroscopic analysis revealed **P1** and **P2** contained 5 mol% pendent azobenzene and α-CD functionalities, respectively (**Figure S2a** and **S2b**, respectively).

The stimuli-responsive supramolecular DCPs were subsequently prepared using sacrificial mesoporous silica (MS) templates with different diameters (340, 460, and 825 nm). The MS templates possessed a bimodal pore structure (2-4 and 10-50 nm pores, as measured by nitrogen sorption) (**Figure S3**), and were synthesized according to previously reported methods.[45-46] Solution state CAP_{ROMP} was used to cross-link the

pHEAm macrocross-linkers **P1** and **P2** (**Scheme 1**) from the initiator functionalized MS templates. To introduce initiating groups, the MS templates were first coated with an allyl-functional poly(ethylene imine) (PEI), followed by cross-metathesis with the ruthenium (Ru) metathesis catalyst **C1**. To maximise non-covalent cross-linking between **P1** and **P2** *via* inclusion complexation between the pendant α-CD and azobenzene moieties prior to covalent cross-linking on to the particles, they were combined in a degassed aqueous solution (1 mM in 50 mM $CuSO_4$ aqueous solution) in equimolar amounts for 30 min. The reversible complexation and decomplexation between α-CD and azobenzene derivatives upon exposure to visible and UV light respectively has been widely reported.[28, 47-50] Commonly, Rotating-frame Overhauser Effect Spectroscopy (ROESY) is used to study correlation peaks indicative of inclusion complexation. Whereas *trans* azobenzene forms a complex with CD to give a correlation peak, UV-mediated isomerisation to the *cis* isomer results in decomplexation and the disappearance of these peaks.[28] This is attributed to the *cis* isomer being too bulky to be accommodated in the CD cavity.[47-50] However, in this study, ROESY could not be utilised to observe these correlations as the mol% of CD and azobenzene moieties are small (5 mol%), making detection of correlation peaks at concentrations relevant to particle assembly difficult.

Dynamic light scattering (DLS) measurements of the **P1**/**P2** supramolecular cross-linked complex revealed a broad peak with multiple shoulders corresponding to an average hydrodynamic diameter ($D_{H,av}$) of 19.5 nm (SI, **Figure S4a**). In contrast, individual solutions of **P1** and **P2** provided $D_{H,av}$ of ~ 10 nm (**Figure S4b** and **c**, respectively). These results indicate the formation of larger aggregates *via* inclusion complexation, and the solution was subsequently added to the **C1**-functionalized MS particles. The relatively small diameter of the P1/P2 supramolecular complex was expected

to facilitate infiltration of the complex into the 10-50 nm diameter pores of the Si templates (**Figure S3**). Once the inclusion complexes come into contact with the initiator functionalized surfaces of the MS particles, covalent cross-linking occurs *via* CAP_{ROMP} to lock the complexes into the particle template. After 24 h the reaction was stopped by repeatedly washing the polymer coated MS particles with Milli-Q water containing di(ethylene glycol) vinyl ether to remove the Ru catalyst. Thermal gravimetric analysis (TGA) of the inclusion complex loaded 825 nm diameter templates after covalent cross-linking revealed that by mass, ~28 wt% consisted of the P1/P2 complex (**Figure S5**). Finally, the MS particle templates were dissolved using buffered hydrofluoric acid to afford the replica DCPs. Unfortunately, attempts to quantify the cross-linking density were unsuccessful and are the subject of ongoing studies

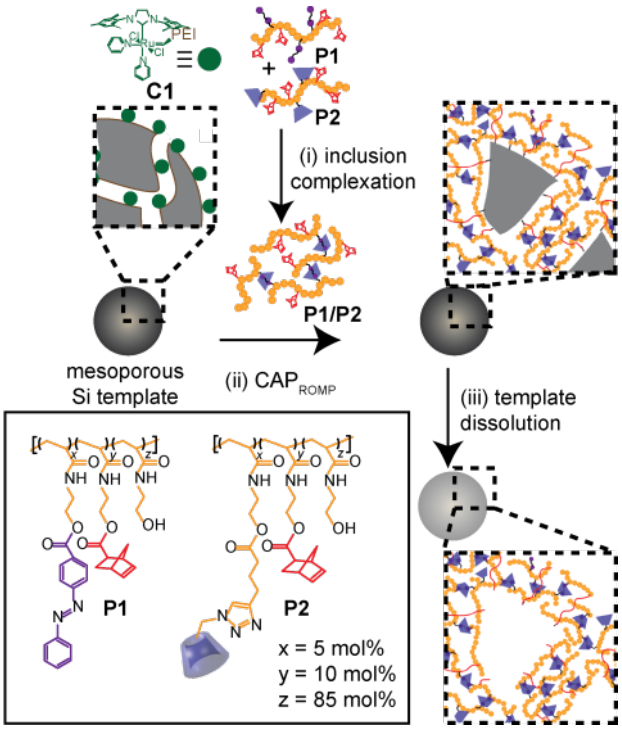

Scheme 1. Schematic illustration showing the formation of dual cross-linked particles (DCPs) *via* a three-step approach: (i) inclusion complexation of the macrocross-linkers

followed by (ii) solution state CAP_{ROMP}, and (iii) subsequent template removal. The macrocross-linkers (**P1** and **P2**) used in this study are shown in the inset.

The DCPs are denoted as DCP_{825}, DCP_{460} and DCP_{340}, according to the MS templates from which they were synthesized. Transmission electron microscopy (TEM) and optical microscopy images of the DCPs (**Figure 1a-c** and **d-f**, respectively) revealed discrete particles, confirming that the CAP_{ROMP} process was surface initiated by the immobilized catalyst **C1**. Statistical analysis of size measurements obtained from TEM imaging (**Figure 1a-c**) revealed the replica DCP_{825}, DCP_{460} and DCP_{340} particles had average particle diameters (D_{av}^{TEM}) of 1220 ± 100, 630 ± 70 and 338 ± 110 nm, respectively (**Figure S6**). DLS measurements of DCP_{825}, DCP_{460} and DCP_{340} in water provided $D_{H,av}$ values of 820, 436 and 378 nm, respectively (**Figure 1g-i**). The larger measurements obtained from TEM images are attributed to the particles generally assuming a 'flattened' conformation when deposited on planar substrates. This phenomenon is commonly observed when imaging soft and deformable polymeric particles and capsules using dry-state TEM.[51-52]

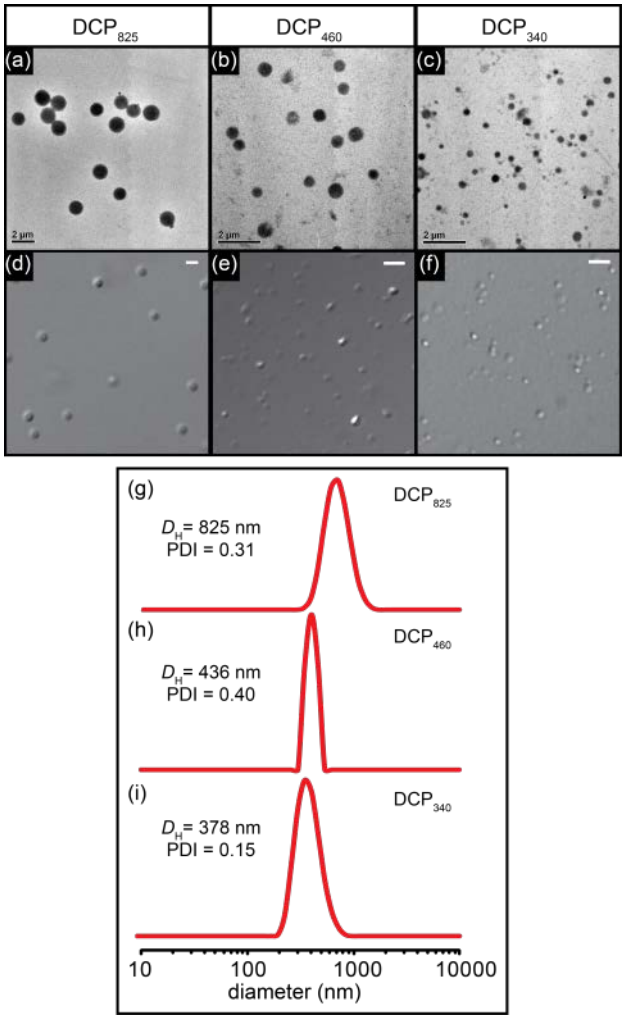

Figure 1. DCPs after template dissolution obtained from different sized MS templates as observed by **(a-c)** TEM and **(d-f)** optical microscopy. Scale bars are all 2 µm. **(g-i)** Size distribution (number %) of the DCPs in water as measured by DLS.

Size measurements of the DCPs were also conducted on air-dried samples using atomic force microscopy (AFM). Aqueous DCP solutions (5 µL, 25 mg.mL^{-1}) were drop-casted onto clean Si wafers and left to air-dry for 12 h before AFM analysis. Distinct particles with spherical morphologies could be seen for all DCPs in both the height and amplitude profiles (**Figure 2a** and **b**, respectively). Using the height profile of different areas, statistical analysis of the DCPs was conducted to measure the average particle diameter (D_{av}^{AFM}) and height (H_{av}^{AFM}). Analysis of DCP_{825} images yielded a D_{av}^{AFM} of 1.98 ± 0.35

μm (**Figure 2c**), which is significantly larger than the values obtained by DLS ($D_{H,av}$ = 0.82 μm) and TEM (D_{av}^{TEM} = 1.22 μm) (**Figure 1g** and **Figure S6a**, respectively). This discrepancy is attributed to the tendency of the particles to assume an even more flattened conformation when air-dried on the planar substrates, as implied by the comparatively low particle heights (DCP_{825} H_{av}^{AFM} = 90.4 ± 22 nm, **Figure 2f**) and when compared to their hydrated measurement by DLS (DCP_{825} $D_{H,av}$ = 820 nm, **Figure 2a**). This trend was also observed throughout the entire series of DCPs. For example, AFM analysis of DCP_{460} revealed a D_{av}^{AFM} of 1.54 ± 0.20 μm and a H_{av}^{AFM} of 23.0 ± 8.8 nm (Fig. 2d and g, respectively), whilst in the hydrated state, DLS measurements revealed a $D_{H,av}$ of 436 nm (**Figure 1h**). Likewise, DCP_{340} had a D_{av}^{AFM} of 0.75 ± 0.08 μm and H_{av}^{AFM} of 89.6 ± 17.2 nm (**Figure 2e** and **h**, respectively), whilst DLS measurements provided a $D_{H,av}$ of 378 nm (**Figure 1i**).

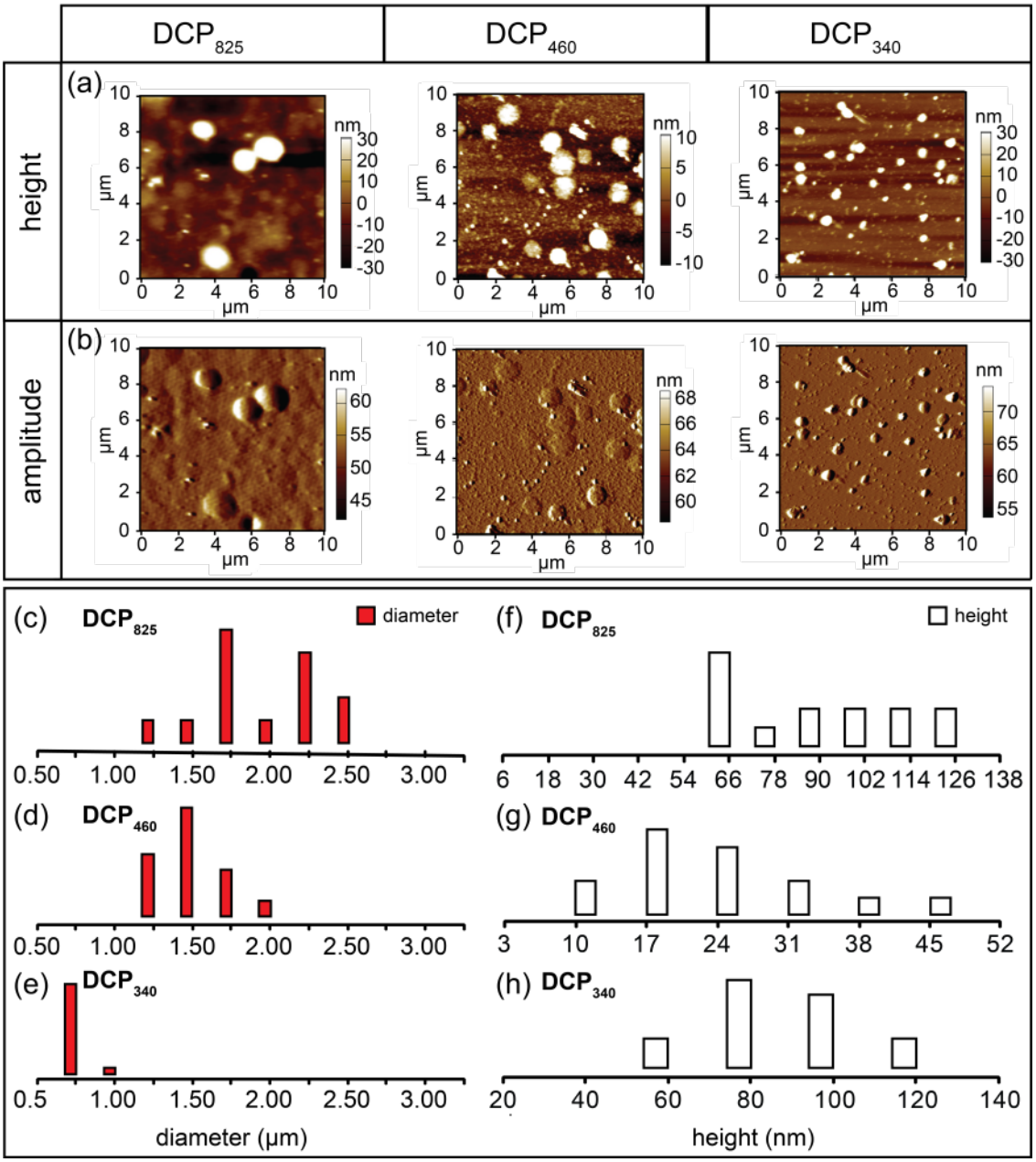

Figure 2. AFM images of air-dried DCP_{825}, DCP_{460} and DCP_{340} casted on Si wafers; **(a)** height profile and **(b)** amplitude trace. Statistical evaluation of the **(c-e)** diameter and **(f-h)** height of the DCPs determined using the height profile at different areas.

By combining the photo-responsive nature of azobenzene derivatives with the ability of α-CDs to selectively form reversible interactions with only the *trans* isomer,[48] the DCPs were designed to have stimuli-responsive properties in the form of particle expansion

when exposed to UV light. Photo-irradiation (λ = 365 nm) of DCP solutions for 15 min resulted in the *trans* to *cis* isomerism of the azobenzene moieties (**Scheme 2**), which drives decomplexation of the CD-azobenzene inclusion complexes, and leads to a decrease in the overall cross-linking density. As a consequence, the DCPs increase in size and permeability (**Scheme 2**). The ability to remotely control the cross-linking density of the particles with on-demand expansion potentially provides new avenues for the use of CD-based supramolecular DCPs in various applications, including on-demand delivery, molecular trapping, and controlled catalysis.

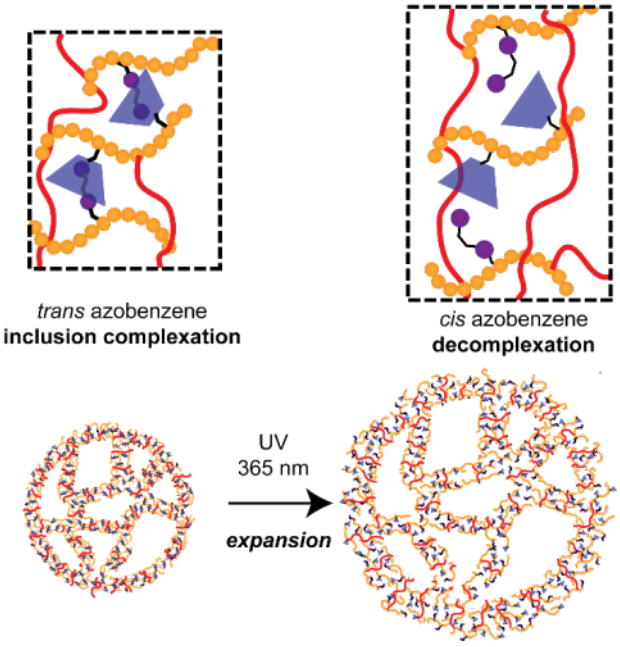

Scheme 2. Graphical illustration of the UV light (λ = 365 nm) initiated expansion of the dual cross-linked particles (DCPs) in aqueous media. Photo-irradiation induces a *trans* to *cis* isomerism of the azobenzene moieties, thus initiating decomplexation of the inclusion complexes, and resulting in particle expansion.

The extent of photo-initiated expansion was investigated for each of the different sized DCPs following exposure to UV light for 15 min. TEM and optical microscopy images of

the DCPs post-irradiation confirmed significant increases in DCP size (**Figure 3a-c** and **Figure S7**, respectively). TEM imaging revealed a decrease in particle contrast post-irradiation (**Figure 3a-c**), which is attributed to a decrease in the total cross-linking density of the DCPs induced by the decomplexation between the CD and azobenzene moieties. Statistical analysis of the TEM images of the irradiated DPCs revealed D_{av}^{TEM} values of 2069 ± 250, 840 ± 130, and 434 ± 60 nm for DCP_{825}, DCP_{460} and DCP_{340}, respectively (**Figure S8**). DLS measurements were also conducted to determine complementary size measurements post-irradiation (**Figure 3d-f**). Using DLS and TEM measurements before and after UV treatment the percentage increase was calculated (**Figure 3g**). DLS measurements of DCP_{825} post-irradiation revealed a $D_{H.av}$ value of 1560 nm, as compared to 820 nm before irradiation (**Figure 3d**); this correlates to an increase in size of ~190%. TEM measurements also provided a comparable value of ~170 % (**Figure 3g**).

The extent of expansion (i.e., change in DCP size before and after UV irradiation) was also shown to be dependent on the DCP size, with smaller particles displaying a less significant increase in size upon irradiation; DCP_{460} and DCP_{340} increased ~130 % and 120 %, respectively (**Figure 3g**). It is hypothesized that the smaller DCPs display a lower expansion due to a higher cross-linking density, resulting from the initial cross-linking process. To confirm that the UV-initiated expansion was solely attributed to the decomplexation of the CD-azobenzene inclusion complexes, control replica particles prepared from pHEAm macrocross-linkers (no inclusion complex) with the same mol% pendant norbornene groups were exposed to UV light. DLS analysis of the control particles (particles prepared solely *via* covalent cross-linking) before and after 15 min of UV irradiation revealed no change in particle size, thus confirming that the expansion of the DCPs results from CD-based decomplexation (**Figure S9**).

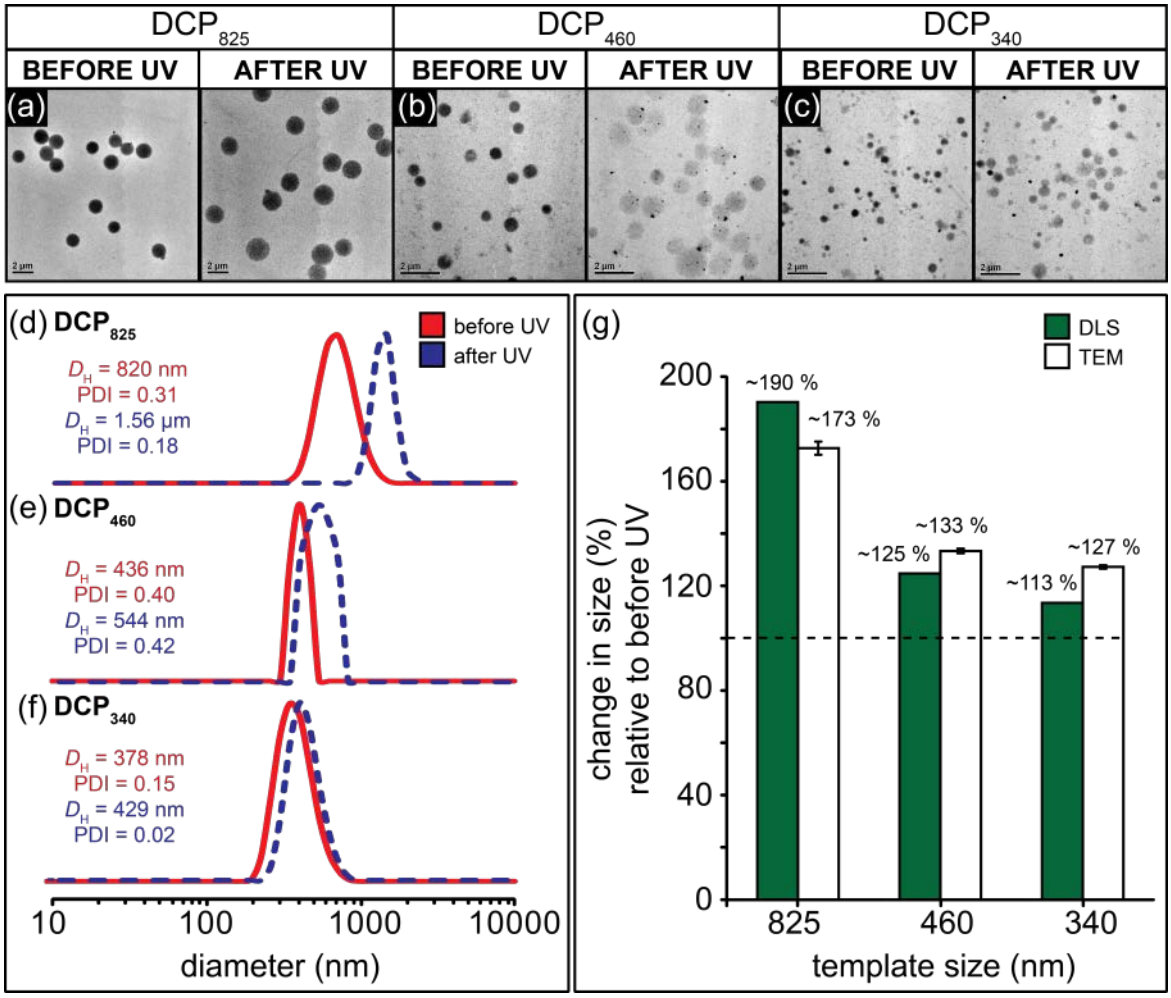

Figure 3. (a-c) TEM images of DCP_{825}, DCP_{460} and DCP_{340} before and after UV treatment (λ = 365 nm). Scale bars are all 2 µm. DLS (number) profiles before (solid trace) and after (dotted trace) UV irradiation of **(d)** DCP_{825}, **(e)** DCP_{460} and (f) DCP_{340}. **(g)** Change in size (%) of the DCPs after UV irradiation relative to measurements taken before UV irradiation as determined from DLS (filled bars) and TEM (un-filled bars) measurements.

The morphology of the DCPs before and after UV irradiation was studied *via* AFM in the dry-state. Aqueous solutions (5 µL, 25 mg mL^{-1}) of the DCPs were drop-casted onto Si wafers and irradiated with UV light (λ = 365 nm) for 15 min before allowing the solvent

to air-dry for AFM analysis. All DCPs after UV irradiation showed a decrease in particle height and an increase in diameter, as observed in the amplitude profiles (**Figure 4-c**), which is consistent with a decrease in cross-linking and the formation of softer and more deformable particles. The extent of particle deformation was further confirmed by statistically analyzing the respective diameters and height of the DCPs in different scanning areas using AFM-generated height profiles (**Figure 4d-i**). The change in particle diameter was most pronounced for DCP_{825} (~3 times larger than DCP_{825} without UV irradiation) compared to DCP_{460} (~1.6 times) and DCP_{340} (~1.4 times) (**Figure 4d-f**). This trend further suggests that DCPs formed using smaller templates have higher covalent cross-linking density, making them inherently less deformable.

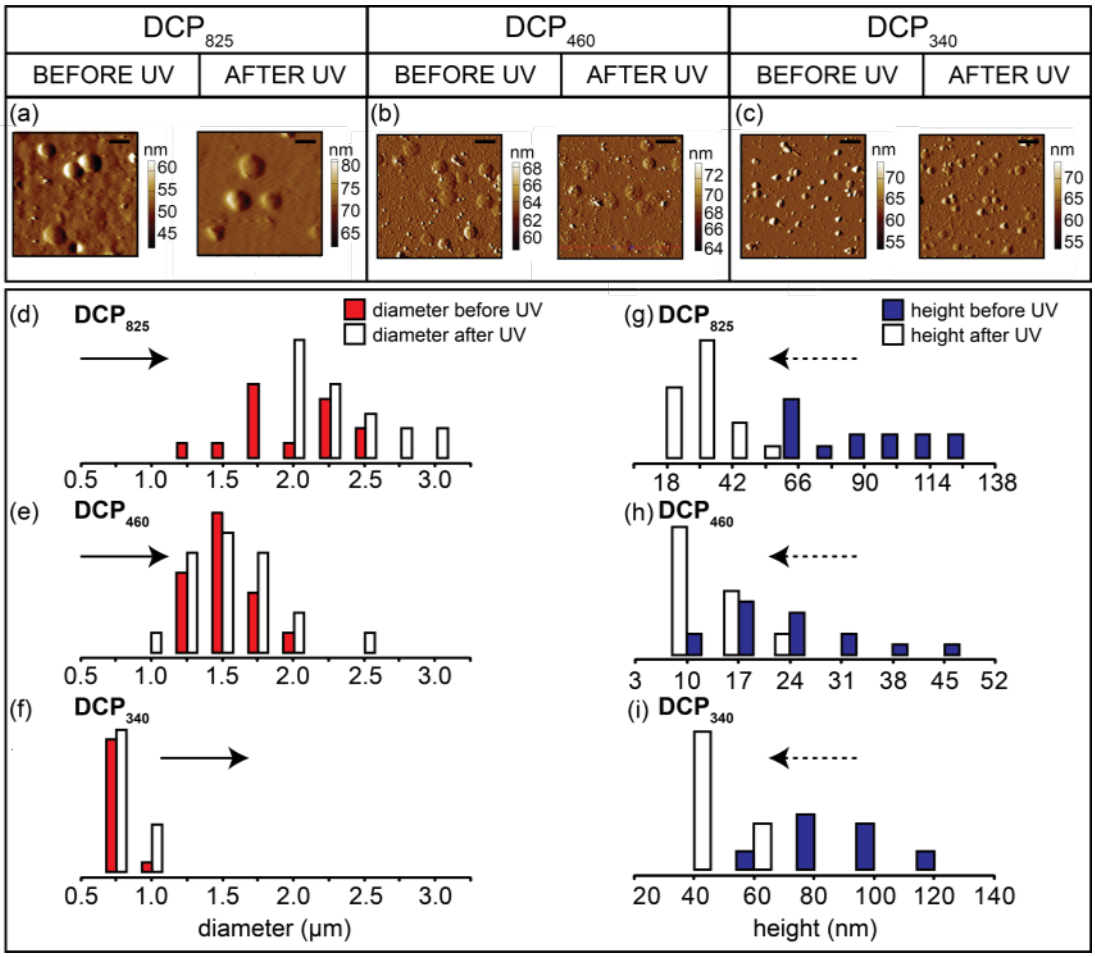

Figure 4. (a-c) AFM amplitude profiles (10 × 10 μm) of air-dried DCPs before and after UV irradiation. Scale bars are all 2 μm. Statistical evaluation of the **(d-f)** diameter and **(g-i)** height of the DCPs before and after UV irradiation.

The DCPs are expected to possess a porous structure as replicated from the MS templates. Upon UV-initiated expansion of the DCPs it is reasonable to assume that the pores increase in size due to a decrease in cross-linking density. The ability to externally trigger an increase in pore size upon UV irradiation allows DCPs to be used as stimuli-responsive delivery vehicles. To demonstrate the feasibility of this concept, fluorescein isothiocyanate (FITC)-labelled dextrans with different molecular weights (250, 500 and 2000 kDa) were used as model payloads. Aqueous solutions of FITC-dextran (100 μL, 0.5 mg mL^{-1}) and DCP_{825} (20 μL, 0.8 mg mL^{-1}) were combined and left to incubate for 10 min before fluorescence microscopy imaging. Before UV irradiation, it was found that DCP_{825} was completely permeable to FITC-dextrans with molecular weights up to 500 kDa and D_H ~29 nm[53] (**Figure 5a** and **Figure S10**). The DCP's ability to efficiently trap the model biomacromolecule was demonstrated using UV spectroscopy; the aqueous solution containing 500 kDa FITC-dextran and DCP_{825} was centrifuged and the supernatant collected for analysis. Both UV spectroscopy and digital images of the supernatant *versus* an aqueous solution with the same 500 kDa FITC-dextran concentration in the absence of the DCPs revealed a high infiltration efficiency (~93%) and a very high loading of 75 wt% (1:3 w/w DCP:dextran) (**Figure S11a-b**). This trend also held true of the lower molecular weight 250 kDa FITC-dextran, which exhibited an entrapment efficiency of ~80 % and a loading of 70 wt% (1: 2.5 w/w DCP:dextran) (**Figure S11c-d**). When FITC-dextran with a molecular weight of 2000 kDa was used,

the FITC-dextran was preferentially located within the periphery of the DCPs (**Figure 5e**), which is attributed to the dextran (D_H = 54 nm)[53] blocking the pores of the DCPs near the particle surface. This phenomenon was further explored *via* fluorescence microscopy where the fluorescence of the 2000 kDa FITC-dextran could be predominantly observed around the cornea of particles. Furthermore, AFM amplitude profiles, revealed that dextran loaded DPCs displayed dry-state morphologies characteristic of "vesicles", whereby the walls are generally observed to be higher than the core (**Figure 5g**). The height profiles of individual particles showed that the 'walls' of the FITC-dextran entrapped DCP_{825} were ~ 13-23 nm thicker than the 'core' (**Figure 5i**). The ability to trap macromolecules with high efficiency implies that the DCPs observe strong interactions with dextran and potential size selectivity making them excellent candidates for macromolecular entrapment and isolation.

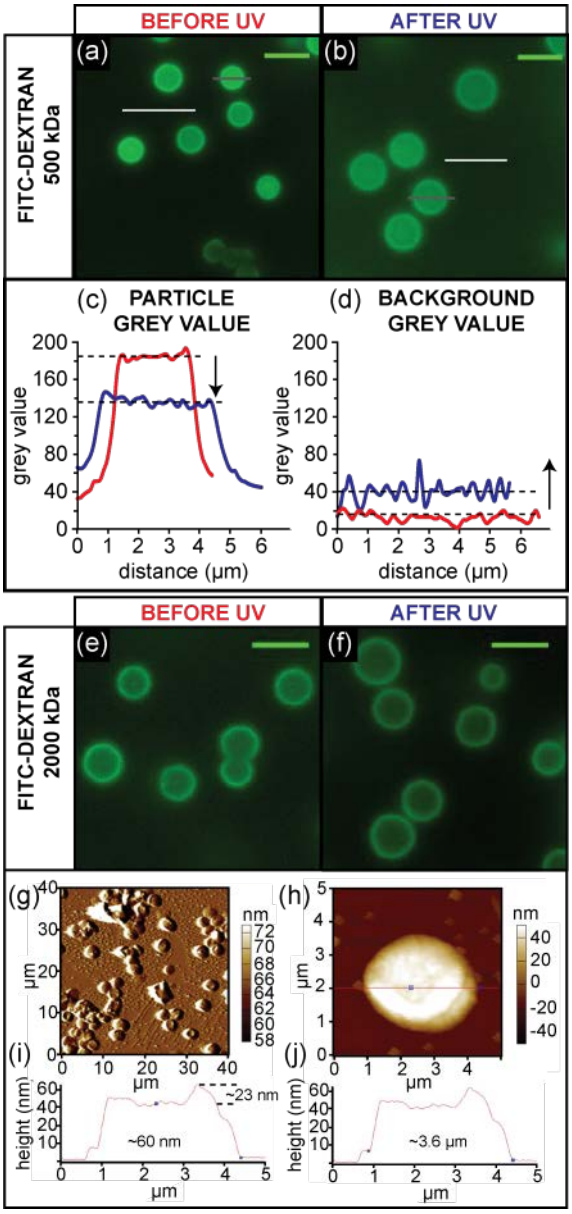

Figure 5. Confocal fluorescent microscopy images of DCP_{825} incubated with various molecular weights of FITC-dextran **(a, e)** before and **(b, f)** after UV irradiation. Scale bars are all 5 μm. Fluorescent intensity profiles of **(c)** DCP_{825} with FITC-dextran 500 kDa before (red trace) and after (blue trace) UV irradiation and **(d)** the background intensity profiles before (red trace) and after (blue trace) UV irradiation. AFM microscopy of air-dried DCP_{825} pre-incubated with 2000 kDa FITC-dextran; **(g)** amplitude and **(h)** height profiles, and **(i, j)** z-profiles showing height ~60 nm and width ~3.6 μm.

Release of the entrapped FITC-dextran (500 kDa) was subsequently initiated by exposing the loaded DCP_{825} to UV light (λ = 365 nm) for 15 min. Fluorescence microscopy revealed a decrease in particle fluorescent intensity consistent with the release of FITC-dextran (**Figure 5a** and **b**, before and after irradiation). The extent of release (~ 38-45% after 15 min of UV irradiation), was determined by measuring the grey values of the particles, and the background before and after irradiation (**Figure 5c** and **d**, respectively). Interestingly, the real-time particle expansion and payload release could be monitored using time-lapse fluorescent microscopy as the wavelength cut-off of the filter was low enough to allow UV light (λ = 365 nm) from the source to activate the particles, resulting in particle expansion. This phenomenon could be observed *via* time-lapse fluorescence microscopy where UV-initiated de-cross-linking result in migration of the fluorescent dextran from the core of the particles towards the outer surfaces (SI, **Figure S12** and **Video S1**). By evaluating each time-lapse microscopy frame, the release profile was determined by evaluating the fluorescent intensities of the FITC-dextran loaded DCP_{825} during UV irradiation. Within 1 s of irradiation, ~50 % of the dextran was released, highlighting the rapid burst release profile of these particles (**Figure 6**).

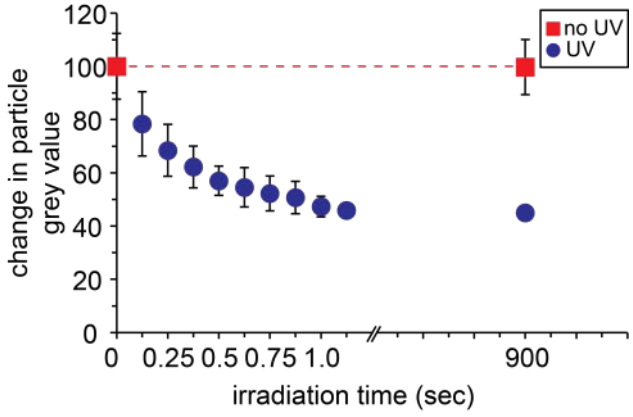

Figure 6. Release profile of 500 kDa FTIC-dextran from DCP_{825} versus irradiation time during UV irradiation (circles) and without irradiation (squares).

The release of 2000 kDa FITC-dextan from DCP_{825} was also observed *via* time-lapse fluorescence microscopy. Whereas before irradiation the 2000 kDa FITC-dextran was predominately located at the particle periphery, time-lapse images revealed that UV irradiation resulted in lower than expected particle expansion and release of the payload. This is possibly due to the large dextran molecules impeding particle expansion through strong intermolecular interactions (**Video S2**). As the release of the payload can be directly related to the cross-linking density and the molecular weight of the payload, by simply tailoring the irradiation intensity and careful selection of cargo the release rate of payloads may potentially be controlled, thus allowing for both burst and sustained release mechanisms.

Although CD-azobenzene complexes are well known to observe reversibility – decomplexation through *trans* to *cis* isomerism of the azobenzene moiety upon irradiation with UV light (365 nm) and recomplexation through *cis* to *trans* isomerism upon exposure to visible light (430 nm)[47-50] – in this system, exposure of the swollen DCPs to visible light did not result in any noticeable changes in the particle size. This is attributed to the high water solubility of the polymeric backbone (i.e., pHEAm) and the conformational restrictions imposed by the cross-links. When the DCPs are exposed to UV light, decomplexation leads to a reduction in the non-covalent cross-links, allowing the polymer chains to relax and adopt a lower energy solvated conformation, leading to particle swelling. Therefore, upon exposure to visible light there is no driving force for the polymer chains to reform the conformationally

restricting noncovalent cross-links that would be required for the DCPs to collapse and shrink.

The cytotoxicity of the DCPs was evaluated by measuring cell viability using a 3-(4,5-dimethylthiaol-2-yl)-2,5-di-phenyl-tetrazolium bromide (MTT) assay against HeLa cells; negligible influence on cell viability was observed at particle-to-cell ratios of up to 100:1 (**Figure 7**), which is comparable to other systems used for drug delivery.[58,59] For biomedical applications, it is anticipated that the DCPs would be degradable as previous studies have shown that the serum enzymes in biological media are capable of ester hydrolysis.[34, 54]

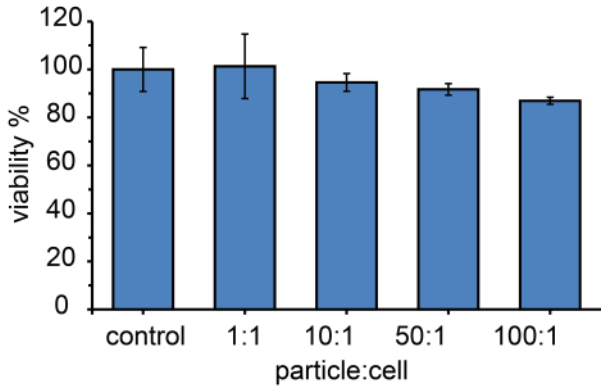

Figure 7. Cell viability assay performed on HeLa cells in the presence of DCP_{825} at different dosages. Cell viability was measured by MTT assay after 24 h incubation at 37 °C. Experiments were conducted in triplicate.

Conclusion

In this study, the combination of CAP_{ROMP} and CD-based host-guest interactions were used to engineer stimuli-responsive dual cross-linked particles (DCPs). In this process, reversible non-covalent cross-linking was formed through CD-azobenzene host-guest interactions, whilst irreversible covalent cross-linking was provided by CAP_{ROMP}. The use of sacrificial mesoporous silica templates with different diameters provided access to DCPs with different diameters and UV-responsive characteristics. The DCPs displayed payload size selectivity and could be loaded with large amounts of dextran (70-75 wt%). By exposing the DCPs to short bursts (1 s) of UV light, *trans* to *cis* isomerism of the azobenzene moieties could be induced. This resulted in the disruption of the non-covalent cross-links without particle degradation. After UV irradiation, highly deformable particles with increased permeability were obtained. The photo-triggered de-cross-linking was shown to induce burst release of dextran, with ~50 % released within 1 s. In this study, the use of UV radiation at 365 nm was used to trigger *trans* to *cis* isomerism of the complexed azobenzene moieties. Since this is within the UVA band, direct sunlight can be used as a stimulus to trigger non-covalent decross-linking. This advantage allows the particles to be used in various applications where the low intensities of UV light (provided by sunlight) can be directly used to control the release of cargo, without the presence of particle degradation products. For example, nutrient and pesticide release for agriculture and environmental control, and as components in food packaging for the release of antibacterial or antifungal agents.

Experimental

1. Experimental section

1.1 Materials:

N-(2-Hydroxyethyl)acrylamide (HEAm, 97%), sodium azide (NaN_3, 99.9%), 5-norbornene-2-carboxylic acid (mixture of *endo* and exo, 98%), 5-hexynoic acid (97%), 4-(phenylazo)benzoic acid (98%), di(ethylene glycol) vinyl ether (98%), poly(ethylene imine) (PEI) (M_w ~25.0 kDa), fluorescein-5(6)-isothiocyanate (FITC, ≥ 90 %), dibutyltin dilaurate (95%), fluorescein isothiocyanate-dextrin (FITC-dextran, M_w = 250 kDa, 500 kDa and 2000 kDa), hydrofluoric acid (48 wt% in H_2O), tetraethyl orthosilicate (TEOS), poly(acrylic acid) (PAA, Mw ~250 kDa, 35 wt% solution in water), cetyltrimethylammonium bromide (CTAB), and 3-(4,5-dimethylthiaol-2-yl)-2,5-diphenyltetrazolium bromide (MTT) were purchased from Sigma-Aldrich and used as received. Mono-6-*O*-(*p*-toluenesulfonyl)-α-cyclodextrin (85%, TCI), magnesium sulphate ($MgSO_4$) (anhydrous, Merck), 4-(dimethylamino)pyridine (DMAP, 99%, Fluka), *N*-(3-(dimethylamino)propyl)-*N*-ethylcarbodiimide hydrochloride (EDCI, 98+%, Acros Organics), *N*,*N*-dimethylformamide (DMF, anhydrous 99.8%, Acros Organics), *N*,*N*-dimethylacetamide (DMAc, anhydrous 99.8%, Acros Organics), 2,2'-azobis(2-methylpropionitrile) (AIBN) (98%, Acros Organics) were all used as received. Diethyl ether (DEE), methanol (MeOH), dimethylsulfoxide (DMSO) and acetone were obtained from Chem-Supply and used as received. Anhydrous and deoxygenated dicholoromethane (DCM) and tetrahydrofuran (THF) were obtained by distillation under argon from CaH_2 and sodium benzophenone ketyl, respectively. Alexa fluor® 488 NHS ester was obtained from Life Technologies. Metathesis catalyst $(IMesH_2)(Cl_2)(C_5H_5N)_2Ru{=}CHPh$ (**C1**) was prepared from the 2nd generation Grubbs

catalyst (Aldrich), as described in the literature.[26] The mesoporous silica (MS) templates was prepared from previously published reports in the literature.[45-46] Deuterated dimethylsulfoxide (d_6-DMSO) was obtained from Cambridge Isotope Laboratories and used as received. High-purity water with a resistivity greater than 18 MΩ.cm was obtained from an in-line Millipore RiOs/Origin water purification system.

1.2 Methods:

Synthesis of mono-6-azido-α-cyclodextrin

Mono-6-*O*-(*p*-toluenesulfonyl)-α-cyclodextrin (500 mg, 0.44 mmol, 1 equiv.) and sodium azide (289 mg, 4.44 mmol, 10 equiv.) were dissolved in anhydrous DMAc (10 mL) and the reaction mixture was continuously stirred at 50 °C for 48 h. The crude reaction mixture was concentrated *in vacuo* (0.1 mbar, 60°C), redissolved in DMAc (3 mL) and precipitated into acetone (30 mL × 3). Subsequently, the product was collected by centrifugation and dried *in vacuo* (0.1 mbar, 60°C) to obtain a white solid, 411 mg (82 %). ^{1}H NMR (400 MHz, d_6-DMSO): δ_H 3.27-3.43 (*m*, 12H, C**H**O), 3.57-3.83 (*m*, 24H, C**H**OH, C**H**O & CHC**H**$_2$OH), 4.50-4.60 (*m*, 5H, CH$_2$O**H**), 4.76-4.85 (*s,* 6H, -OC**H**), 5.39-5.57 (*m*, 12H, -CO**H)** ppm. MALDI-ToF MS [M + Na$^+$]: 1020.8 Da.

Synthesis of poly(N-hydoxylethyl acrylamide), pHEAm

N-(2-Hydoxyethyl) acrylamide (HEAm) (1 mL, 9.65 mmol, 50 equiv) and AIBN (31.69 mg, 0.19 mmol, 1 equiv.) were dissolved in anhydrous DMAc (10 mL) and the mixture was degassed for 1 h under nitrogen atmosphere. Subsequently the mixture was heated to 70 °C and stirred continuously for 5 h. The crude reaction mixture was then

precipitated into DEE (100 mL × 2), collected by centrifugation and dried *in vacuo* (0.1 mbar) to afford pHEAm as a tacky clear solid, 839 g (84 %). ^{1}H NMR (400 MHz, d_6-DMSO): δ_H 1.25-1.53 (*m*, 3H, C***H***$_2$C***H****(C=O)*CH$_2$ repeat unit), 3.34 (*s*, 3H, O=CN***H***C***H***$_2$), 4.77-5.04 (*m*, 1H, -CH$_2$O***H***), 7.63 (*s,* 1H, O=CN**H**CH$_2$) ppm. GPC (aqueous): M_n = 12.9 kDa, $Đ$ = 1.84.

Synthesis of norbornene functionalized pHEAm macrocross-linker (poly(hydoxyethyl)acrylamide-co-(2-(acryloyloxy)ethyl bicyclo[2.2.1]hept-5-ene-2-carboxylate))), ***P0***

pHEAm (500 mg, 0.02 mmol, 1 equiv.), EDCI (83.77 mg, 0.432 mmol, 24 equiv.) and DMAP (2.64 mg, 0.022 mmol, 1 equiv.) were dissolved in DMF (5 mL). 5-Norbornene-2-carboxylic acid (60 mg, 0.432 mmol, 24 equiv.) was then added and the reaction mixture was stirred at room temperature for 16 h. The crude reaction mixture was then concentrated *in vacuo* (0.1 mbar, 60 °C), redissolved in MeOH (3 mL) and precipitated into DEE (30 mL). The product was collected by centrifugation and then lypholised to obtain **P0** as a tacky solid, 0.50 g (89 %). ^{1}H NMR (400 MHz, d_6-DMSO): δ_H 1.25-1.53 (*m*, 3H, C**H**$_2$C***H****(C=O)*CH$_2$ repeat unit), 3.34 (*s*, 3H, O=CN**H**C**H**$_2$), 4.77-5.04 (*m*, 1H, -CH$_2$O**H**), 5.86-6.13 (*m*, 2H, **H**C=(C**H**)CH), 7.63 (*s,* 1H, O=CN**H**CH$_2$) ppm.

Synthesis of azobenzene-*co*-norbornene *functionalized pHEAm macrocross-linker* ***P1***

P0 (300 mg, 0.01 mmol, 1 equiv.), EDCI (5.23 mg, 0.03 mmol, 2.5 equiv.), DMAP (1.61 mg, 0.01 mmol, 1.2 equiv.) and 4-(phenylazo)benzoic acid (6.10 mg, 0.03 mmol, 2.5 equiv.) were dissolved in DMF (3 mL) and continuously stirred at room temperature for 16 h. The crude reaction mixture was then precipitated into DEE (30 mL × 2). The

product was collected by centrifugation and dried *in vacuo* (0.1 mbar, 60 °C) to obtain **P1** as a tacky orange solid, 255 mg (85 %). ^{1}H NMR (400 MHz, d_6-DMSO): δ_H 1.25-1.53 (*m*, 3H, C**H**$_2$C***H****(C=O)*CH$_2$ repeat unit), 3.34 (*s*, 3H, O=CN**H**C**H**$_2$), 3.91-4.07 (*m*, 2H, CH$_2$C**H**$_2$O(C=O)Ar), 4.77-5.04 (*m*, 1H, -CH$_2$O**H**), 5.86-6.13 (*m*, 2H, **H**C=(C**H**)CH), 7.63 (*s,* 1H, O=CN**H**CH$_2$) ppm.

Synthesis of alkyne-*co*-norbornene *functionalized pHEAm macrocross-linker*

P0 (300 mg, 0.01 mmol, 1 equiv.), EDCI (5.23 mg, 0.03 mmol, 2.5 equiv.), DMAP (1.61 mg, 0.01 mmol, 1.2 equiv.) and 5-hexynoic acid (5.05 mg, 0.03 mmol, 2.5 equiv.) were dissolved in DMF (3 mL) and continuously stirred at room temperature for 16 h. The crude reaction mixture was then precipitated into DEE (30 mL × 2). The product was collected by centrifugation and dried *in vacuo* (0.1 mbar, 60 °C) to obtain a tacky solid, 256 mg (85 %). ^{1}H NMR (400 MHz, d_6-DMSO): δ_H 1.25-1.53 (*m*, 3H, C**H**$_2$C***H****(C=O)*CH$_2$ repeat unit), 2.38-2.44 (m, 2H, C**H**$_2$CH$_2$OC=O), 3.27-3.43 (m, 6H, O=CC**H**$_2$C**H**$_2$C**H**$_2$), 3.34 (*s*, 3H, O=CN**H**C**H**$_2$), 4.77-5.04 (*m*, 1H, -CH$_2$O**H**), 5.86-6.13 (*m*, 2H, **H**C=(C**H**)CH), 7.63 (*s,* 1H, O=CN**H**CH$_2$) ppm.

Synthesis of α-cyclodextrin-*co*-norbornene *functionalized pHEAm macrocross-linker* ***P2***

Alkyne-*co*-norbornene functionalized pHEAm (200 mg, 0.007 mmol, 1 equiv.), mono-6-azido-α-cyclodextrin (35.9 mg, 0.036 mmol, 5 equiv.) and PMDETA (12.5 mg, 0.072 mmol, 10 equiv.) were dissolved in DMF (2 mL) and degassed under a N_2 atmosphere for 30 min. Subsequently, copper(I) iodide (13.71 mg, 0.072 mmol, 10 equiv.) was added and the reaction mixture was continuously stirred under N_2 atmosphere for 48 h. The crude reaction mixture was then dialyzed (MWCO = 3500 g. mol^{-1}) against EDTA

solution (0.04 M), followed by MeOH for 2 days to remove the copper complexes. The solution was then concentrated *in vacuo* (0.1 mbar, 60 °C) and precipitated into DEE (30 mL) to obtain **P2** as a white tacky solid, 168 mg (78 %). ^{1}H NMR (400 MHz, d_6-DMSO): δ_H 1.25-1.53 (*m*, 3H, C**H**$_2$C***H****(C=O)***CH$_2$ repeat unit), 3.34 (*s*, 3H, O=CN**H**C**H**$_2$), 3.94-4.10 (m, 2H, CH$_2$C**H**$_2$OC=O), 4.77-5.04 (*m*, 7H, -CH$_2$O**H** & CO**H**), 5.37-5.62 (*m*, 12H, CO**H** & CO**H**), 5.86-6.13 (*m*, 2H, **H**C=(C**H**)CH), 7.63 (*s,* 1H, O=CN**H**CH$_2$) ppm.

1.3 Particle preparation

*Inclusion complexation of macrocross-linkers **P1** and **P2***

Inclusion complexation between the macrocross-linkers **P1** and **P2** was achieved by continuously stirring a degassed aqueous solution (1 mM in 50 mM $CuSO_4$) of **P1** and **P2** in equimolar amounts for 30 min.

Assembly of dual cross-linked particles

All particle experiments were conducted in individual 1.5 mL microcentifuge tubes. Particles (0.5 wt% solution) functionalized with catalyst **C1** (details of this functionalization are provided in the previously published literature[1]) were combined with a 1 mL CAP-active macrocross-linker (pre-inclusion complex of **P1**/**P2**) solution (1 mM in 50 mM $CuSO_4$) in a microcentifuge tube. The mixture was agitated with a Thermomixer at room temperature for 24 h and the CAP_{ROMP} process was terminated by the addition of excess di(ethylene glycol) vinyl ether (100 µL). After 10 min the particles were isolated by centrifugation, washed with Milli-Q water (3 × 1 mL) and soaked in Milli-Q water (1 mL) for 24 h prior to analysis. The silica templates were dissolved using

2 M HF/8 M NH_4F solution. *Caution! HF is highly toxic. Extreme care should be taken when handling HF solution.*

Fluorescent labelling of dual cross-linked particles

Once the cross-linked particles were fabricated and suspended in Milli-Q water (2.5 mg mL^{-1}) they were washed with distilled THF (1 mL × 3). The particles were then re-suspended in dry THF (150 μL). 50 μL of dibutylin dilaurate (0.5 mg mL^{-1}) and 100 μL of Alexa flour 488 (0.5 mg mL^{-1}) in dry THF were added into the particle suspension. The mixture was subsequently agitated with a Thermomixer at room temperature for 24 h before the particles were washed with THF (1 mL × 3) and re-suspended in 1 mL of Milli-Q water.

1.4 Cytotoxicity Assay

MTT assays were performed to check the toxicity of the polymer particles against HeLa cells according to the previously established method.[55] HeLa cells were seeded in a 96 well plate at a population of 10^4 cells per well (200 μL medium per well). After incubation with the particles at various capsule-to-cell ratios for 24 h, 20 μL of MTT (5 mg mL^{-1}) was added to each well. Following 4 h incubation at 37 °C (5% CO_2), the media were carefully removed and the resulting formazan in cells was dissolved in DMSO. The percentage of cell viability was determined from the absorption at 570 nm.

1.6 Measurements:

Gel Permeation Chromatography (GPC)

Polymer molecular weight distributions was measured *via* aqueous-phase GPC using a Shimadzu liquid chromatography system equipped with a Shimadzu RID-10 refractometer (λ = 633 nm), and three Waters Ultrahydrogel columns in series ((i) 250 Å porosity, 6 μm diameter bead size; (ii) and (iii) linear, 10 μm diameter bead size), operating at room temperature. The eluent was Milli-Q water containing 20% v/v acetonitrile and 0.1% w/v TFA at a flow rate of 1 mL min^{-1}. The molecular weight characteristics of the analytes were determined by comparison to narrow molecular weight poly(ethylene glycol) standards. All samples were filtered through a 0.45 μm nylon filters prior to injection.

Nuclear Magnetic Resonance (NMR) Spectroscopy

^{1}H NMR spectroscopy was conducted on a Varian Unity 400 MHz spectrometer operating at 400 MHz, using the deuterated solvent as reference and a sample concentration of ~ 20 mg mL^{-1}.

Atomic force microscopy (AFM)

AFM images of air-dried particles on silicon wafers were acquired with an MFP-3D Asylum Research instrument. Typical scans were conducted in AC mode with ultrasharp SiN gold-coated cantilevers (MikroMasch, Bulgaria). Image processing and height profile analyses were performed using the Nanoscope and Igor Pro software programs, respectively.

Dynamic light scattering (DLS)

Dynamic light scattering (DLS) measurements were performed on a Wyatt DynaPro NanoStar instrument fitted with a 120 mW Ga-As laser operating at 658 nm; 100 mW was delivered to the sample cell. Analysis was performed at an angle of 90° and at constant temperatures of 25 ± 0.01 °C.

Fluorescence microscopy

Fluorescence images were taken on an inverted Olympus IX71 microscope equipped with a 60× objective lens (Olympus UPFL20/0.5 NA, W.D. 1.6). A CCD camera was mounted on the left-hand port of the microscope. Fluorescence images were illuminated with an X-cite module. Deconvolution fluorescence microscopy was performed on a DeltaVision (Applied Precision) microscope with a 60× 1.42 NA oil objective and a standard FITC/TRITC/CY5 filter set. Images were processed with ImageJ.

Transmission Electron Microscopy (TEM)

TEM images were taken with a Philips CM120 BioTWIN TEM at an operating voltage of 120 kV. Samples of the particles were air-dried on a carbon-coated Formvar film mounted on 300 mesh copper grids (ProSciTech, Australia).

UV-Visible Spectroscopy

UV–Vis analysis was performed on a Shimadzu UV–Vis Scanning Spectrophotometer (UV-2101 PC) using quartz cuvettes.

ASSOCIATED CONTENT Supporting Information Available: Additional information. This material is available free of charge via the internet at **http://pubs.acs.org**.

References

(1) Esser-Kahn, A. P.; Odom, S. A.; Sottos, N. R.; White, S. R.; Moore, J. S. Triggered Release from Polymer Capsules. *Macromolecules* **2011,** *44*, 5539-5553.

(2) Stuart, M. A. C.; Huck, W. T.; Genzer, J.; Müller, M.; Ober, C.; Stamm, M.; Sukhorukov, G. B.; Szleifer, I.; Tsukruk, V. V.; Urban, M. Emerging Applications of Stimuli-Responsive Polymer Materials. *Nat. Mater.* **2010,** *9*, 101-113.

(3) Kromidas, L.; Perrier, E.; Flanagan, J.; Rivero, R.; Bonnet, I. Release of Antimicrobial Actives from Microcapsules by the Action of Axillary Bacteria. *Int. J Cosmetic Sci.* **2006,** *28*, 103-108.

(4) Goldberg, M. E.; Kellner, D. M.; Lew, C. W.; Lamb, C. S. Encapsulated Antiperspirant Salts and Deodorant/Antiperspirants. Google Patents: **1993**.

(5) Friedman, S.; Mualem, Y. Diffusion of Fertilizers from Controlled-Release Sources Uniformly Distributed in Soil. *Fert. Res.* **1994,** *39*, 19-30.

(6) Peteu, S. F.; Oancea, F.; Sicuia, O. A.; Constantinescu, F.; Dinu, S. Responsive Polymers for Crop Protection. *Polymers* **2010,** *2*, 229-251.

(7) De Koker, S.; Hoogenboom, R.; De Geest, B. G. Polymeric Multilayer Capsules for Drug Delivery. *Chem. Soc. Rev.* **2012,** *41*, 2867-2884.

(8) Ruiz-Esparza, G. U.; Wu, S.; Segura-Ibarra, V.; Cara, F. E.; Evans, K. W.; Milosevic, M.; Ziemys, A.; Kojic, M.; Meric-Bernstam, F.; Ferrari, M.; Blanco, E. Polymer Nanoparticles Encased in a Cyclodextrin Complex Shell for Potential Site- and Sequence-Specific Drug Release. *Adv.Funct. Mater.* **2014,** *24*, 4753-4761.

(9) Städler, B.; Chandrawati, R.; Price, A. D.; Chong, S. F.; Breheney, K.; Postma, A.; Connal, L. A.; Zelikin, A. N.; Caruso, F. A Microreactor with Thousands of Subcompartments: Enzyme-Loaded Liposomes within Polymer Capsules. *Angew. Chem.* **2009,** *121*, 4423-4426.

(10) Price, A. D.; Zelikin, A. N.; Wang, Y.; Caruso, F. Triggered Enzymatic Degradation of DNA within Selectively Permeable Polymer Capsule Microreactors. *Angew. Chem. Int. Ed.* **2009,** *48*, 329-332.

(11) Such, G. K.; Tjipto, E.; Postma, A.; Johnston, A. P.; Caruso, F. Ultrathin Responsive Polymer Click Capsules. *Nano Lett.* **2007,** *7*, 1706-1710.

(12) Delcea, M.; Möhwald, H.; Skirtach, A. G. Stimuli-Responsive LbL Capsules and Nanoshells for Drug Delivery. *Adv. Drug Delivery Rev.* **2011,** *63*, 730-747.

(13) Pelton, R., Temperature-Sensitive Aqueous Microgels. *Adv. Colloid Interface Sci.* **2000,** *85*, 1-33.

(14) Kuckling, D.; Vo, C. D.; Wohlrab, S. E. Preparation of Nanogels with Temperature-Responsive Core and pH-Responsive Arms by Photo-cross-linking. *Langmuir* **2002,** *18* , 4263-4269.

(15) Onaca, O.; Enea, R.; Hughes, D. W.; Meier, W. Stimuli-Responsive Polymersomes as Nanocarriers for Drug and Gene Delivery. *Macromol. Biosci.* **2009,** *9*, 129-139.

(16) Zhao, M.; Biswas, A.; Hu, B.; Joo, K.-I.; Wang, P.; Gu, Z.; Tang, Y. Redox-Responsive Nanocapsules for Intracellular Protein Delivery. *Biomaterials* **2011,** *32*, 5223-5230.

(17) Bédard, M. F.; De Geest, B. G.; Skirtach, A. G.; Möhwald, H.; Sukhorukov, G. B. Polymeric Microcapsules with Light Responsive Properties for Encapsulation and Release. *Adv. Colloid Interface Sci.* **2010,** *158*, 2-14.

(18) Kang, H.; Trondoli, A. C.; Zhu, G.; Chen, Y.; Chang, Y.-J.; Liu, H.; Huang, Y.-F.; Zhang, X.; Tan, W. Near-Infrared Light-Responsive Core–Shell Nanogels for Targeted Drug Delivery. *ACS Nano* **2011,** *5*, 5094-5099.

(19) Zelikin, A. N.; Quinn, J. F.; Caruso, F. Disulfide Cross-Linked Polymer Capsules: en route to Biodeconstructible Systems. *Biomacromolecules* **2006,** *7*, 27-30.

(20) Liang, K.; Such, G. K.; Zhu, Z.; Yan, Y.; Lomas, H.; Caruso, F. Charge-Shifting Click Capsules with Dual-Responsive Cargo Release Mechanisms. *Adv. Mater.* **2011,** *23*, H273-H277.

(21) Kempe, K.; Noi, K. F.; Ng, S. L.; Müllner, M.; Caruso, F. Multilayered polymer capsules with switchable permeability. *Polymer* **2014,** *55*, 6451-6459.

(22) Goh, T. K.; Guntari, S. N.; Ochs, C. J.; Blencowe, A.; Mertz, D.; Connal, L. A.; Such, G. K.; Qiao, G. G.; Caruso, F. Nanoengineered Films via Surface-Confined Continuous Assembly of Polymers. *Small* **2011,** *7*, 2863-2867.

(23) Guntari, S. N.; Goh, T. K.; Blencowe, A.; Wong, E. H. H.; Caruso, F.; Qiao, G. G. Factors Influencing the Growth and Topography of Nanoscale Films fabricated by ROMP-mediated Continuous Assembly of Polymers. *Polym. Chem.* **2013,** *4*, 68-75.

(24) Guntari, S. N.; Khin, A. C. H.; Wong, E. H. H.; Goh, T. K.; Blencowe, A.; Caruso, F.; Qiao, G. G. (Super)hydrophobic and Multilayered Amphiphilic Films Prepared by Continuous Assembly of Polymers. *Adv. Funct. Mat.* **2013,** *23*, 5159-5166.

(25) Guntari, S. N.; Nam, E.; Pranata, N. N.; Chia, K.; Wong, E. H.; Blencowe, A.; Goh, T. K.; Caruso, F.; Qiao, G. G. Fabrication of Chiral Stationary Phases via Continuous Assembly of Polymers for Resolution of Enantiomers by Liquid Chromatography. *Macromol. Mater. Eng.* **2014,** *299*, 1285-1291.

(26) Guntari, S. N.; Wong, E. H. H.; Goh, T. K.; Chandrawati, R.; Blencowe, A.; Caruso, F.; Qiao, G. G. Low-Fouling, Biospecific Films Prepared by the Continuous Assembly of Polymers. *Biomacromolecules* **2013,** *14*, 2477-2483.

(27) Wong, E. H. H.; van Koeverden, M. P.; Nam, E.; Guntari, S. N.; Wibowo, S. H.; Blencowe, A.; Caruso, F.; Qiao, G. G. Assembly of Nanostructured Films with Hydrophobic Subcompartments via Continuous Assembly of Polymers. *Macromolecules* **2013,** *46*, 7789-7796.

(28) Tan, S.; Wong, E. H. H.; Fu, Q.; Ren, J. M.; Sulistio, A.; Ladewig, K.; Blencowe, A.; Qiao, G. G. Azobenzene-Functionalised Core Cross-Linked Star Polymers and their Host–Guest Interactions. *Aust. J Chem.* **2014,** *67*, 173-178.

(29) Tan, S.; Ladewig, K.; Fu, Q.; Blencowe, A.; Qiao, G. G. Cyclodextrin-Based Supramolecular Assemblies and Hydrogels: Recent Advances and Future Perspectives. *Macromol. Rapid Commun.* **2014,** *35*, 1166-1184.

(30) Araki, J.; Ito, K. Recent Advances in the Preparation of Cyclodextrin-Based Polyrotaxanes and their Applications to Soft Materials. *Soft Matter* **2007,** *3*, 1456-1473.

(31) van de Manakker, F.; Vermonden, T.; van Nostrum, C. F.; Hennink, W. E. Cyclodextrin-Based Polymeric Materials: Synthesis, Properties, and Pharmaceutical/Biomedical Applications. *Biomacromolecules* **2009,** *10*, 3157-3175.

(32) Mellet, C. O.; Fernandez, J. M. G.; Benito, J. M. Cyclodextrin-based Gene Delivery Systems. *Chem. Soc. Rev.* **2011,** *40*, 1586-1608.

(33) Harada, A.; Takashima, Y.; Nakahata, M. Supramolecular Polymeric Materials via Cyclodextrin–Guest Interactions. *Acc. Chem. Res.* **2014,** *47*, 2128-2140.

(34) Tan, S.; Nam, E.; Cui, J.; Xu, C.; Fu, Q.; Ren, J. M.; Wong, E. H. H.; Ladewig, K.; Caruso, F.; Blencowe, A.; Qiao, G. G. Fabrication of Ultra-Thin Polyrotaxane-Based Films via Solid-State Continuous Assembly of Polymers. *Chem. Commun.* **2015,** *51*, 2025-2028.

(35) Tan, S.; Fu, Q.; Scofield, J. M.; Kim, J.; Gurr, P. A.; Ladewig, K.; Blencowe, A.; Qiao, G. G., Cyclodextrin-based Supramolecular Polymeric Nanoparticles for Next Generation Gas Separation Membranes. *J. Mater. Chem. A* **2015,** *3*, 14876-14886.

(36) Harada, A.; Takashima, Y.; Yamaguchi, H., Cyclodextrin-based Supramolecular Polymers. *Chem. Soc. Rev.* **2009,** *38*, 875-882.

(37) Fu, Q.; Ren, J. M.; Qiao, G. G., Synthesis of Novel Cylindrical Bottlebrush Polypseudorotaxane via Inclusion Complexation of High Density Poly([varepsilon]-caprolactone) Bottlebrush Polymer and α-Cyclodextrins. *Polym. Chem.* **2012,** *3*, 343-351.

(38) Takashima, Y.; Sahara, T.; Sekine, T.; Kakuta, T.; Nakahata, M.; Otsubo, M.; Kobayashi, Y.; Harada, A. Supramolecular Adhesives to Hard Surfaces: Adhesion Between Host Hydrogels and Guest Glass Substrates Through Molecular Recognition. *Macromol. Rapid Commun.* **2014,** *35*, 1646-1652.

(39) Nakamura, T.; Takashima, Y.; Hashidzume, A.; Yamaguchi, H.; Harada, A., A Metal–Ion-Responsive Adhesive Material via Switching of Molecular Recognition Properties. *Nat. Commun.* **2014,** *5*, 1-9.

(40) Nakahata, M.; Takashima, Y.; Yamaguchi, H.; Harada, A. Redox-Responsive Self-Healing Materials Formed from Host–Guest Polymers. *Nat. Commun.* **2011,** *2*, 511.

(41) Kakuta, T.; Takashima, Y.; Nakahata, M.; Otsubo, M.; Yamaguchi, H.; Harada, A. Preorganized Hydrogel: Self-Healing Properties of Supramolecular Hydrogels Formed by Polymerization of Host–Guest-Monomers that Contain Cyclodextrins and Hydrophobic Guest Groups. *Adv. Mater.* **2013,** *25*, 2849-2853.

(42) Nakahata, M.; Takashima, Y.; Hashidzume, A.; Harada, A. Redox-Generated Mechanical Motion of a Supramolecular Polymeric Actuator Based on Host–Guest Interactions. *Angew. Chem.Int. Ed.* **2013,** *52*, 5731-5735.

(43) Katagiri, K.; Koumoto, K.; Iseya, S.; Sakai, M.; Matsuda, A.; Caruso, F. Tunable UV-Responsive Organic– Inorganic Hybrid Capsules. *Chem. Mater.* **2008,** *21*, 195-197.

(44) Zhao, C.; Zheng, J. Synthesis and Characterization of Poly(N-hydroxyethylacrylamide) for Long-Term Antifouling Ability. *Biomacromolecules* **2011,** *12*, 4071-4079.

(45) Cui, J.; De Rose, R.; Alt, K.; Alcantara, S.; Paterson, B. M.; Liang, K.; Hu, M.; Richardson, J. J.; Yan, Y.; Jeffery, C. M.; Price, R. I.; Peter, K.; Hagemeyer, C. E.; Donnelly, P. S.; Kent, S. J.; Caruso, F. Engineering Poly(ethylene glycol) Particles for Improved Biodistribution. *ACS Nano* **2015,** *9*, 1571-1580.

(46) Cui, J.; De Rose, R.; Best, J. P.; Johnston, A. P.; Alcantara, S.; Liang, K.; Such, G. K.; Kent, S. J.; Caruso, F. Mechanically Tunable, Self-Adjuvanting Nanoengineered Polypeptide Particles. *Adv. Mater.* **2013,** *25*, 3468-3472.

(47) Yamaguchi, H.; Kobayashi, Y.; Kobayashi, R.; Takashima, Y.; Hashidzume, A.; Harada, A., Photoswitchable Gel Assembly based on Molecular Recognition. *Nat. Comm.***2012,** *3*, 603.

(48) Liao, X.; Chen, G.; Liu, X.; Chen, W.; Chen, F.; Jiang, M. Photoresponsive Pseudopolyrotaxane Hydrogels Based on Competition of Host–Guest Interactions. *Angew. Chem. Int. Ed.* **2010,** *49*, 4409-4413.

(49) Wang, Y.; Ma, N.; Wang, Z.; Zhang, X. Photocontrolled Reversible Supramolecular Assemblies of an Azobenzene-Containing Surfactant with α-Cyclodextrin. *Angew. Chem. Int. Ed.* **2007,** *46*, 2823-2826.

(50) Tamesue, S.; Takashima, Y.; Yamaguchi, H.; Shinkai, S.; Harada, A. Photoswitchable Supramolecular Hydrogels formed by Cyclodextrins and Azobenzene Polymers. *Angew. Chem.***2010,** *122*, 7623-7626.

(51) Liang, K.; Such, G. K.; Zhu, Z.; Dodds, S. J.; Johnston, A. P. R.; Cui, J.; Ejima, H.; Caruso, F. Engineering Cellular Degradation of Multilayered Capsules through Controlled Cross-Linking. *ACS Nano* **2012,** *6*, 10186-10194.

(52) Leung, M. K.; Such, G. K.; Johnston, A. P.; Biswas, D. P.; Zhu, Z.; Yan, Y.; Lutz, J. F.; Caruso, F. Assembly and Degradation of Low-Fouling Click-Functionalized Poly (ethylene glycol)-Based Multilayer Films and Capsules. *Small* **2011,** *7*, 1075-1085.

(53) Schmidt, S.; Behra, M.; Uhlig, K.; Madaboosi, N.; Hartmann, L.; Duschl, C.; Volodkin, D., Mesoporous Protein Particles Through Colloidal CaCO3 Templates. *Adv. Funct. Mater.* **2013,** *23*, 116-123.

(54) Tan, S.; Blencowe, A.; Ladewig, K.; Qiao, G. G., A Novel One-Pot Approach towards Dynamically Cross-Linked Hydrogels. *Soft Matter* **2013,** *9*, 5239-5250.

(55) Liang, K.; Such, G. K.; Johnston, A. P. R.; Zhu, Z.; Ejima, H.; Richardson, J. J.; Cui, J.; Caruso, F. Endocytic pH-Triggered Degradation of Nanoengineered Multilayer Capsules. *Adv. Mater.* **2014,** *26*, 1901-1905.

Table of Contents

Upon photo-irradiation, instantaneous burst release of cargo from polymeric particles could be engineered without particle degradation. This is achieved *via* a dual cross-linking concept where cyclodextrin chemistry provides the non-covalent cross-links whilst continuous assembly of polymers mediates the covalent cross-links. The dual cross-linked particles observe efficient infiltration and high loadings of dextran; a hydrophilic (bio)-macromolecule. Upon short exposure to UV light, increased particle permeability and burst release of cargo could be directly visualized by time-lapse fluorescent microscopy.

Author/s:
Tan, S; Cui, J; Fu, Q; Nam, E; Ladewig, K; Ren, JM; Wong, EHH; Caruso, F; Blencowe, A; Qiao, GG

Title:
Photocontrolled Cargo Release from Dual Cross-Linked Polymer Particles

Date:
2016-03-09

Citation:
Tan, S., Cui, J., Fu, Q., Nam, E., Ladewig, K., Ren, J. M., Wong, E. H. H., Caruso, F., Blencowe, A. & Qiao, G. G. (2016). Photocontrolled Cargo Release from Dual Cross-Linked Polymer Particles. ACS APPLIED MATERIALS & INTERFACES, 8 (9), pp.6219-6228. https://doi.org/10.1021/acsami.5b11186.

Persistent Link:
http://hdl.handle.net/11343/124161

File Description:
Accepted version